EurJIC
European Journal of Inorganic Chemistry

A Journal of ChemPubSoc Europe

Accepted Article

Title: Refinement of the Microwave-Assisted Polyol Process for the Low-Temperature Synthesis of Intermetallic Nanoparticles

Authors: Johannes Teichert, Martin Heise, Jen-Hui Chang, and Michael Ruck

To be cited as: *Eur. J. Inorg. Chem.* 10.1002/ejic.201700966

Link to VoR: http://dx.doi.org/10.1002/ejic.201700966

WILEY-VCH

Refinement of the Microwave-Assisted Polyol Process for the Low-Temperature Synthesis of Intermetallic Nanoparticles

Johannes Teichert,[a] Martin Heise,[a] Jen-Hui Chang[a] and Michael Ruck*[a,b]

Abstract: The microwave-assisted polyol process was applied to synthesize phase-pure micro- or nanocrystalline samples of intermetallic phases in the systems T–M (with T = Co, Ni, Rh, Pd, Ir, Pt and M = Sn, Sb, Pb, Bi). Reaction temperatures range between 240 °C and 300 °C and reaction times of a few minutes up to one hour are sufficient. For the optimization of the syntheses reaction temperature, reaction time, and metal precursors were changed. To obtain phase-pure samples the process was further modified by the addition of potassium hydroxide, oleylamine, or oleic acid. Single-phase powders of a variety of intermetallic compounds were synthesized. Although not stable at the temperature of synthesis, high-temperature phases are accessible as well. The microwave-assisted polyol process opens up the possibility to synthesize intermetallic compounds in a fast and easily applicable one-step route, without the utilization of strong and often toxic reducing agents.

Introduction

Nanomaterials exhibit outstanding properties because of the drastically increased ratio of surface atoms and quantum confinement effects.[1] Among others, nanocrystalline metallic and intermetallic compounds show interesting catalytic, optical, and magnetic properties which open up a broad field for possible applications.[2,3] Commonly, intermetallic compounds are synthesized by high-temperature sintering, melt crystallization, or high-pressure methods.[4] To compensate the slow diffusion in the solid state, these reactions require high temperatures and long annealing times, sometimes up to several months. Crystallization from melt, which is of course also a high-temperature process, usually results in the thermodynamically stable products, although often high-temperature phases can be quenched. Moreover, obtaining single-phase products by means of peritectic or peritectoid phase formation is challenging if not impossible. Finally, the milling of bulk intermetallics to their nanopowders can be a severe problem because they are often either too hard or too soft, and the control of size and morphology of the particles is rather limited.

The polyol process, a solution-based low-temperature method, has been identified as an effective alternative to directly produce micro- or nanocrystals of metallic elements or compounds.[5–7] Reaction temperatures range from room temperature to about 320 °C and reaction times of several minutes up to hours are sufficient. The method is based on the (co-)reduction of metal salts in a polyol (e.g. ethylene glycol, EG), which simultaneously acts as solvent, reducing agent, and surfactant.[8] Depending on the chemical system and the process parameters either mixtures of different metal particles, core-shell particles, gradient crystals, homogeneous alloys, or intermetallics with own structure type result.

The reduction potential of ethylene glycol strongly depends on the temperature. The higher the temperature of the polyol the higher is its ability to reduce metal cations.[9] Nevertheless, not all metal cations can be reduced by the polyol. The polyol process was used to produce nano- and submicrometer particles of the metals Co, Ni, Cu, Ru, Rh, Pd, Ag, Cd, Ir, Pt, Au, Pb, and Bi.[5–7,10–13] It was observed that hydroxide addition often enhances the reducing ability of the polyol. This could be due to the deprotonation of the polyol, which facilitates the electron transfer to the metal cations.[14] Furthermore hydroxide ions can act as ligands and alter the solubility properties and reduction potentials of metal cations. By addition of a stronger reducing agent, e.g. $NaBH_4$ or hydrazine, less noble metals like indium are accessible as well.[15] This is commonly denoted as “modified polyol process”. The synthesis of non-agglomerated particles with controlled size and shape is typically achieved by addition of surfactants like poly(vinylpyrrolidone)[16] or oleylamine[17].

Next to the synthesis of metallic elements, the polyol process was widely applied to the production of bimetallic alloys as well as core-shell nanoparticles.[8] Only a few publications cover the synthesis of intermetallic compounds by the polyol process. Schaak et al. performed systematic studies on $NaBH_4$-modified polyol synthesis of binary phases in the systems Au–Cu[18,19], M–Sn[20,21], Pt–M[20] and Co–Sb[20]. Using a multi-step synthesis protocol even ternary phases, namely $AuCuSn_2$ and $AuNiSn_2$, could be accessed.[22,23] The major drawback of these syntheses is the utilization of corrosive and toxic reducing agents. In contrast, polyols itself are biodegradable and exhibit only low to moderate toxicity.[8] Therefore, an unmodified polyol process would be desirable for the synthesis of intermetallic nanoparticles. This has already been achieved for a few compounds, e.g. Pd_3Sn_2[24], Pd_3Pb[25], $PtBi_2$[26], and PtBi[26,27].

In the last years our group has synthesized a variety of binary bismuth-containing intermetallic nanoparticles without the addition of strong reductants by the microwave-assisted polyol process.[28–31] Microwave radiation is an efficient heating source for highly polar solvents like polyols. Because of the unique dielectric heating mechanism from the inside of the reaction

---

[a] Department Chemistry and Food Chemistry, Technische Universität Dresden
01062 Dresden, Germany
E-mail: michael.ruck@tu-dresden.de
https://tu-dresden.de/mn/chemie/ac/ac2/

[b] Max Planck Institute for Chemical Physics of Solids
01187 Dresden, Germany

Supporting information for this article is given via a link at the end of the document.

mixture wall effects can be diminished. High heating rates and a relatively homogenous temperature profile in the reaction vessel lead to short reaction times and a minimum amount of byproducts.[32–34] The commonly applied closed-vessel setup opens up the possibility to work under solvothermal conditions. High yields of phase-pure powders with small particle-size distributions and well-shaped crystallites can been obtained by the microwave-assisted polyol process.

Nanoscaling of intermetallic compounds with this process revealed some remarkable effects on the physical and chemical properties, which shall be demonstrated by three examples. (A) Nanocrystalline $NiBi_3$ exhibits the very rare simultaneous existence of the antagonists superconductivity and ferromagnetism below 4.06 K.[28,35] It has been shown that special surface states in combination with the high specific surface lead to this phenomenon.[36] (B) Phase-pure pseudo-hexagonal shaped nanocrystals of RhBi proved extraordinary catalytic performance in the semi-hydrogenation of acetylene to ethylene with respect to conversion and selectivity.[29] (C) In a reversible process, nanocrystalline $IrBi_3$ activates molecular oxygen from air and intercalates it into its structure, thereby forming the first metallic oxide ion conductor and the first that operates at room temperature.[30] Recently, we showed the potential of the microwave-assisted polyol process in the synthesis of binary Pd–Bi compounds. All phases, including some that are thermodynamically stable only at high temperatures, can be synthesized utilizing a modified polyol process.[31] Potassium hydroxide and surfactants like oleylamine and oleic acid were used to ensure the formation of phase-pure products and to promote the crystallization of uniform well-shaped monodisperse nanoparticles.

In this study we focus on the microwave-assisted polyol process for the synthesis of nanocrystalline intermetallic compounds between electron-rich transition metals *T* (Co, Ni, Rh, Pd, Ir, Pt) and heavy main group elements *M* (Sn, Sb, Pb, Bi). We present an overview of known intermetallic phases in the systems *T*–*M* and established nanoparticle syntheses, show the possibilities given by the microwave-assisted polyol process in the synthesis of phase-pure nanocrystalline powders, and also try to evaluate the limitations of this method. The products were characterized by means of powder X-ray diffraction (PXRD), scanning electron microscopy (SEM), and energy-dispersive X-ray spectroscopy (EDS).

Results and Discussion

By adapting the initial metal ratio, reaction temperature, reaction time, addition of oleylamine and oleic acid, and pH modification by KOH we synthesized pure nanocrystalline samples of as many *T*–*M* binary phases (*T* = Co, Ni, Rh, Pd, Ir, Pt and *M* = Sn, Sb, Pb, Bi) as possible (Table 1). In most cases the molar ratio of the starting materials primarily determines the product formed. Nevertheless, because each binary system revealed its own characteristics, the procedures had to be tested by systematic variation of all synthesis parameters until an optimum was reached. Because of the complexity of the system and the large number of factors that are crucial for high-yield single-phase product formation, these results represent a progress report but cannot provide a general statement to the synthesis of binary intermetallics.

The standard reduction potential can be seen as a rough indicator for the feasibility of the polyol process. The least noble metal which could be produced in boiling ethylene glycol is cobalt (standard potential –0.28 V for Co^{2+}/Co^0). Phase-pure iron microparticles could be produced starting from $FeCl_2$ in strongly alkaline polyol media at relatively low temperatures.[37–39] Fiévet et al. proposed that this is not a reduction reaction but a disproportionation of Fe^{2+} to Fe^{3+} and Fe^0, which also accounts for the low yields obtained.[37] Considering only the standard potential the reduction of all metal cations used in this study should be possible. However, the reduction of antimony(III) (standard potential +0.150 V) as well as tin(II) (standard potential –0.138 V) to the elements proved to be impossible. In preliminary tests microwave treatment up to 300 °C starting from different precursor salts with or without hydroxide addition resulted in clear solutions or precipitation of oxides or alkoxides. Mixtures containing transition metal cations led to the formation of intermetallic *T*–Sb and *T*–Sn compounds. Obviously, not only the standard potentials of the individual metal species but also the free enthalpy of phase formation is important for the "reducibility" of metal cations in polyols. The synthesis of intermetallics with high tin or antimony content was not possible. In contrast, bismuth- and lead-rich phases can easily be obtained. For some systems, namely Co–Sn, Rh–Sn, Ir–Sn, and Ir–Sb, only amorphous or poorly crystalline black powders could be obtained directly from the polyol process. Iridium and rhodium are very noble metals which give rise to rapid nucleation and limited particle growth. Most probably the produced nanoparticles are too small to give intense diffraction signals. For Ir–Sb, it was possible to obtain crystalline $IrSb_2$ by heating raw "$IrSb_3$" nanopowder in an evacuated ampoule. Using the same strategy for tin compounds, oxide impurities were often observed which probably arise from an incomplete reduction.

In the following sections, the features of some individual phase systems will be discussed, ordered by the main group metal *M*. For each system the known intermetallic compounds and established nanoparticle syntheses are presented followed by the synthesis results of the microwave-assisted polyol process.

Synthesis of *T*–Sn phases. The *Ni–Sn* phase diagram comprises the room-temperature phases α-Ni_3Sn, α-Ni_3Sn_2, Ni_3Sn_4 and two high-temperature phases β-Ni_3Sn and β-Ni_3Sn_2.[40] Several syntheses for Ni–Sn nanoparticles were reported. For example, nanocrystalline β-Ni_3Sn_2 was obtained by a co-reduction route of $SnCl_2$ and $NiCl_2$ using $NaBH_4$ in ethanol.[41] This method offered the crystallization of the high temperature phase in form of agglomerated granule-like particles with 30 nm and smaller in diameter. The co-reduction of $SnCl_2$ and $NiCl_2$ or $Ni(OAc)_2$ with $NaBH_4$ in tetraethylene glycol yielded nanocrystalline Ni_3Sn_4.[20,42] The previously unknown compound $NiSn_3$ resulted from the conversion of β-Sn nanocrystals with $NiCl_2$ at 150 °C in tetraethylene glycol using $NaBH_4$ as reducing agent.[21]

Table 1. Summary for the investigated binary phase systems *T–M*. Bold face type indicates phases that were obtained by the microwave-assisted polyol process. Phase-pure products are underlined. For completeness, previously published syntheses of Ni–Bi, Rh–Bi, Pd–Bi, and Ir–Bi compounds are included.[28–31]

System	Phases
Co–Sn	α-Co_3Sn_2, β-Co_3Sn_2, CoSn, $CoSn_2$, α-$CoSn_3$, β-$CoSn_3$
Ni–Sn	α-Ni_3Sn, **β-Ni_3Sn**,α-Ni_3Sn_2, **β-Ni_3Sn_2**, Ni_3Sn_4
Rh–Sn	Rh_2Sn, Rh_3Sn_2, RhSn, α-$RhSn_2$, β-$RhSn_2$, $RhSn_4$
Pd–Sn	Pd_3Sn, **Pd_2Sn**, **$Pd_{20}Sn_{13}$**, γ (≈ $Pd_{65}Sn_{35}$), α-Pd_3Sn_2, β-Pd_3Sn_2, δ (≈ $Pd_{59}Sn_{41}$), **PdSn**, Pd_5Sn_7, $PdSn_2$, $PdSn_3$, $PdSn_4$
Ir–Sn	IrSn, Ir_5Sn_7, $IrSn_2$, Ir_3Sn_7, α-$IrSn_4$, β-$IrSn_4$
Pt–Sn	**Pt_3Sn**, **PtSn**, Pt_2Sn_3, $PtSn_2$, $PtSn_4$
Co–Sb	**CoSb**, α-$CoSb_2$, β-$CoSb_2$, $CoSb_3$
Ni–Sb	**α-Ni_3Sb**, β-Ni_3Sb, **Ni_5Sb_2**, **NiSb**, $NiSb_2$
Rh–Sb	Rh_2Sb, Rh_3Sb_2, **RhSb**, $RhSb_2$, $RhSb_3$
Pd–Sb	Pd_3Sb, **$Pd_{20}Sb_7$**, **Pd_8Sb_3**, Pd_5Sb_2, Pd_2Sb, Pd_5Sb_3, **PdSb**, **$PdSb_2$**
Ir–Sb	IrSb, $IrSb_2$, $IrSb_3$
Pt–Sb	Pt_7Sb, Pt_5Sb, **Pt_3Sb**, **Pt_3Sb_2**, **PtSb**, **$PtSb_2$**
Rh–Pb	Rh_3Pb_2, RhPb, **Rh_4Pb_5**, **$RhPb_2$**, $RhPb_4$
Pd–Pb	**Pd_3Pb**, **α-Pd_5Pb_3**, β-Pd_5Pb_3, **$Pd_{13}Pb_9$**, **PdPb, $PdPb_2$**
Pt–Pb	Pt_3Pb, **PtPb**, **$PtPb_4$**
Ni–Bi	**NiBi**, **$NiBi_3$**
Rh–Bi	**RhBi**, **α-$RhBi_2$**, β-$RhBi_2$, $RhBi_3$, **$RhBi_4$**
Pd–Bi	**Pd_3Bi**, **$Pd_{31}Bi_{12}$**, **Pd_5Bi_2**, $PdBi_{0.6}$, α-PdBi, **β-PdBi**, **γ-PdBi** (metastable), **α-$PdBi_2$**, β-$PdBi_2$
Ir–Bi	**$IrBi_2$**, **$IrBi_3$**
Pt–Bi	**PtBi**, **Pt_2Bi_3**, **α-$PtBi_2$**, **β-$PtBi_2$, γ-$PtBi_2$**

By the microwave-assisted polyol process, we synthesized phase-pure β-Ni_3Sn_2 as intergrown platelets that form spherical agglomerates (desert rose morphology) with diameters of about 100 nm (Figure 1a, b). The crystallization and stabilization of this high-temperature phase takes place by simple usage of ethylene glycol as solvent and reducing agent without utilizing any auxiliary, in contrast to the approaches in literature. Starting with the ratio Ni:Sn = 3:1, also the nickel-rich high-temperature phase β-Ni_3Sn crystallized besides β-Ni_3Sn_2 (Figure S1 in the Supporting Information). We did not observe the formation of Ni_3Sn_4 even with low Ni:Sn starting ratios.

The complex *Pd–Sn* phase diagram comprises eight room-temperature phases (Pd_3Sn, Pd_2Sn, $Pd_{20}Sn_{13}$, α-Pd_3Sn_2, γ-phase ≈ $Pd_{59}Sn_{41}$, PdSn, Pd_5Sn_7, $PdSn_2$, $PdSn_3$, $PdSn_4$) and two high-temperature phases (β-Pd_3Sn_2, δ-phase ≈ $Pd_{65}Sn_{35}$).[43] In previous investigations, nanocrystals of Pd_2Sn[44] and PdSn[21] were synthesized by a modified polyol process using $NaBH_4$ as reducing agent. Pd_3Sn_2 nanoparticles could be obtained by Sun et al. without using an additional reducing agent in EG under solvothermal conditions.[24]The similarity of the powder pattern of $Pd_{20}Sn_{13}$ with the pattern of Pd_3Sn_2 (PDF number 4-801, no crystal structure deposited in the ICSD) and the phase width of $Pd_{20}Sn_{13}$ indicate, that this phase may be the main product in the published synthesis.

We synthesized nanocrystalline samples of Pd_2Sn, $Pd_{20}Sn_{13}$, and PdSn by the microwave-assisted polyol process. Phase-pure Pd_2Sn (Figure 1c) precipitated starting from Pd:Sn ratios 2:1, 3:2, and 1:1. For accessing the compounds $Pd_{20}Sn_{13}$ and PdSn (Figure 1e, g) an initial metal ratio of at least Pd:Sn = 1:2 was necessary. Nanocrystalline $Pd_{20}Sn_{13}$ formed at 240 °C while nanocrystals of PdSn were obtained at 290–300 °C. The co-reduction of Sn^{2+} seems to be favored at higher temperature, in accordance with the general reducibility trend in polyols. The excess of tin cations remained in solution. EDS analyses confirmed the expected compositions of the products Pd_2Sn ($Pd_{66.7}Sn_{33.3}$; measured: $Pd_{67(2)}Sn_{33(2)}$), $Pd_{20}Sn_{13}$ ($Pd_{60.6}Sn_{39.4}$; measured: $Pd_{59(1)}Sn_{41(1)}$), and PdSn (measured: $Pd_{48(1)}Sn_{52(1)}$). SEM measurements revealed highly agglomerated particles in all cases. In samples of Pd_2Sn and $Pd_{20}Sn_{13}$ the average particle size is 50 nm (Figure 1d, f), and in PdSn the largest particles observed have diameters of about 100 nm (Figure 1h). All tested syntheses targeting on the other known phases in this system resulted in the crystallization of only one of the three described phases Pd_2Sn, $Pd_{20}Sn_{13}$, or PdSn.

In the *Pt–Sn* system, the phases Pt_3Sn, PtSn, Pt_2Sn_3, $PtSn_2$, and $PtSn_4$ are known.[45] Several syntheses of nanocrystalline samples in this system are reported in the literature. The synthesis of PtSn by a modified polyol process was done by Schaak et al.[20] A synthesis-screening for nanoscale Pt–Sn compounds was performed with a room-temperature reduction approach by alkali metal borohydrides, revealing the formation of ordered intermetallic nanoparticles for Pt_3Sn and PtSn.[46] Only by further annealing of the as-prepared samples, the tin-rich compounds Pt_2Sn_3, $PtSn_2$, and $PtSn_4$ could be crystallized.

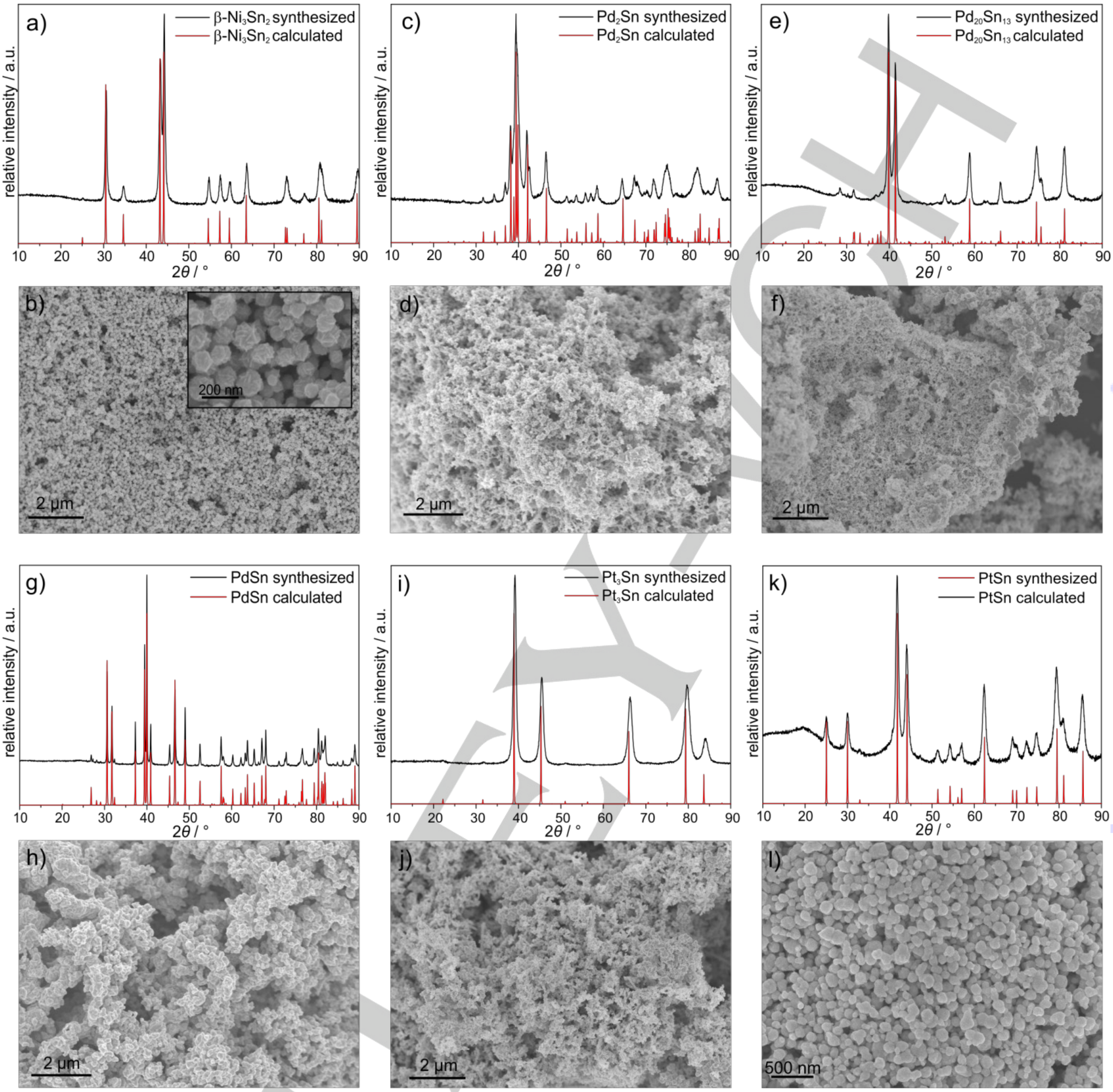

Figure 1. Powder X-ray diffractograms (Cu-$K_{\alpha1}$ radiation) and SEM pictures of (a, b) β-Ni_3Sn_2, (c, d) Pd_2Sn, (e, f) $Pd_{20}Sn_{13}$, (g, h) PdSn, (i, j) Pt_3Sn, and (k, l) PtSn, respectively. XRD shows that the samples are phase-pure. According to the SEM pictures agglomerated nanoparticles were produced. Ni_3Sn_2 particles with desert rose morphology and diameters of about 100 nm were formed by intergrowth of thin platelets (inset in b).

A stepwise injection method at 300 °C using hexadecanediol as the reducing agent gave direct access to nanocrystalline Pt_3Sn, PtSn, and $PtSn_2$.[47] $PtSn_4$ could be accessed directly by controlled oxidation of preformed Zintl clusters with iodine.[48]

Pt_3Sn and PtSn are accessible by the microwave-assisted polyol process. Starting with metal ratio Pt:Sn = 3:1 but also Pt:Sn = 2:1 phase pure Pt_3Sn was produced, according to PXRD (Figure 1i). EDS analyses for the samples with the initial metal ratio Pt:Sn = 3:1 verified the expected composition (measured: $Pt_{77(2)}Sn_{23(2)}$). The product consists of agglomerated nanoparticles with a broad particle size distribution (Figure 1j). For the synthesis of PtSn, an initial excess of tin (Pt:Sn = 1:3) was necessary. According to PXRD phase-pure PtSn was obtained (Figure 1k). The particles have diameters of about 100 nm (Figure 1l).

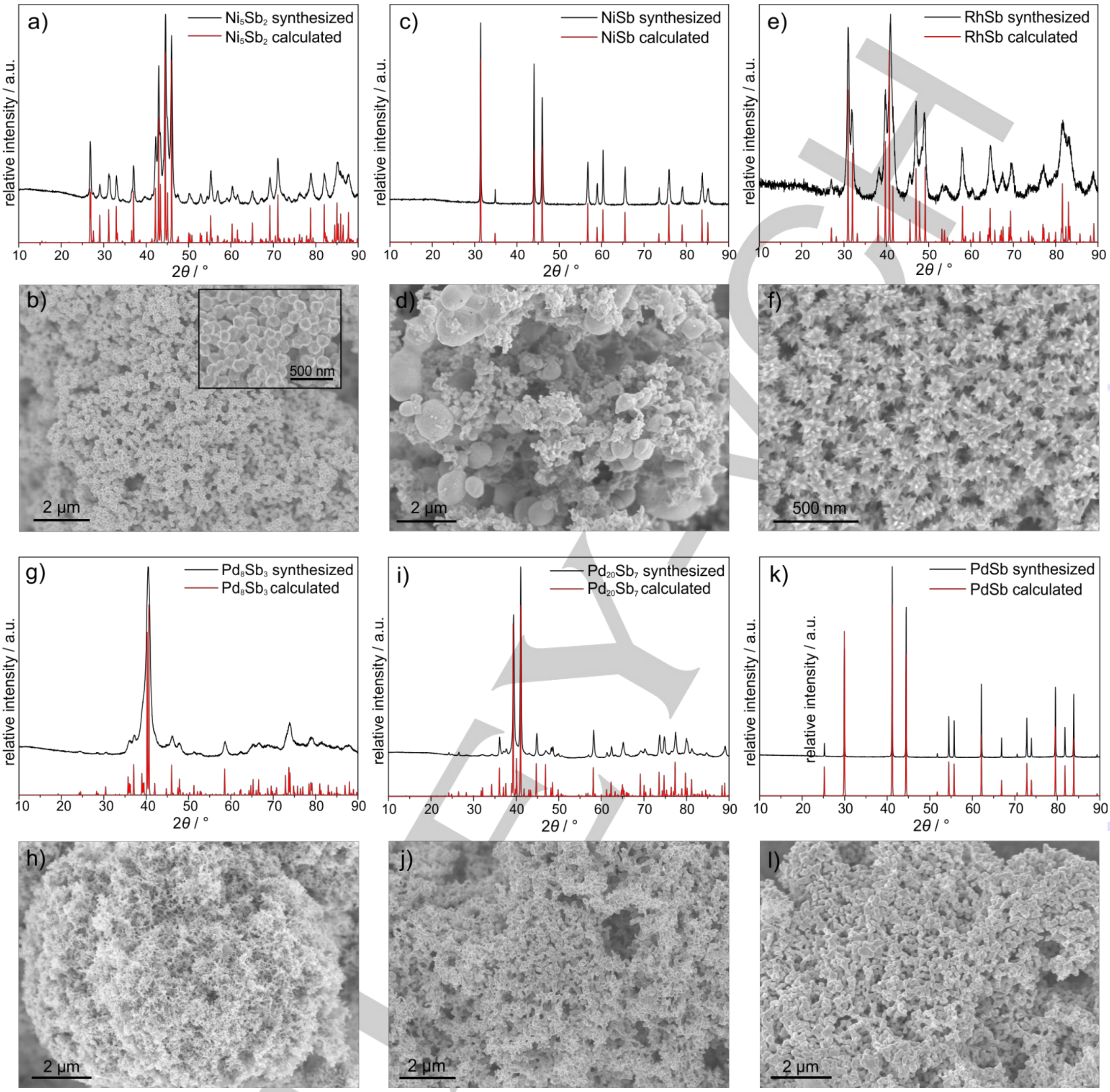

Figure 2. Powder X-ray diffractograms (Cu-$K_{\alpha1}$ radiation) and SEM pictures of (a, b) Ni_5Sb_2, (c, d) NiSn, (e, f) RhSb, (g, h) $Pd_{20}Sb_7$, (i, j) Pd_8Sb_3, and (k, l) PdSb, respectively. XRD shows that the samples are phase-pure. According to the SEM pictures agglomerated nanoparticles were obtained.

Curiously, the calculated yield based on PtSn is 131 %. EDS analysis showed an average product composition $Pt_{31(2)}Sn_{69(2)}$. Most probably, the PtSn nanoparticles are surrounded by amorphous tin or tin oxide. In resistance measurements, pellets of the product showed the behavior of a doped semiconductor, although bulk PtSn is a metallic conductor.Overall, we observed that an initial tin content of less than 50 at.-% always resulted in the formation of “pure” Pt_3Sn, whereas more than 50 at.-% always led to “pure” PtSn. Remarkably, the reduction of both types of metal cations was completely hindered at very high excess of tin, e.g. when starting with the ratio Pt:Sn = 1:8.

Synthesis of *T*–Sb phases. The *Ni–Sb* phase diagram indicates four room-temperature intermetallic phases (α-Ni_3Sb, Ni_5Sb_2 – also denoted as Ni_7Sb_3, NiSb, $NiSb_2$) and the high-temperature phase β-Ni_3Sb.[49] Nanocrystalline Ni–Sb compounds were first produced by co-reduction of $NiCl_2{\cdot}6H_2O$ and $SbCl_3$ in ethanol with zinc or $NaBH_4$ as reducing agents in an autoclave.[50,51] The choice of the reducing agent influenced the product formation. The authors only got access to phase-pure antimony-rich phases, namely NiSb and $NiSb_2$. NiSb can also be obtained by $NaBH_4$ reduction[52] or by heating of pre-synthesized nickel and antimony nanoparticles[53] in tetraethylene glycol. Syntheses of nanocrystalline nickel-rich phases in this system have not been described yet.

By the microwave-assisted polyol process starting from $Ni(OAc)_2$ and $Sb(OAc)_3$ we obtained α-Ni_3Sb, Ni_5Sb_2, and NiSb. α-Ni_3Sb (Figure S3 in the Supporting Information) was synthesized using an excess of nickel in the initial ratio (Ni:Sb = 5:1). As a consequence, crystallization of the solid solution $Ni_{1-x}Sb_x$ ($x \leq 0.05$, i.e. nickel with antimony impurities) occurred. Starting with Ni:Sb = 3:1, mixtures of nanocrystalline Ni_5Sb_2 and NiSb were obtained.

Phase-pure Ni_5Sb_2 (Figure 2a) resulted starting from a Ni:Sb ratio of 5:2 and using some KOH. EDS analyses showed a composition $Ni_{71(2)}Sb_{29(2)}$ (expected: $Ni_{71.4}Sb_{28.6}$). For NiSb (Figure 2c), the initial ratio Ni:Sb = 1:1 was required without further addition of auxiliaries. Adding more $Sb(OAc)_3$ to the starting solution (up to Ni:Sb = 1:4) did not lead to the formation of $NiSb_2$ but of phase-pure NiSb. Excess Sb^{3+} cations remained in solution, which was confirmed by EDS measurements on the resulting powders showing the composition $Ni_{51(1)}Sb_{49(1)}$. The corresponding SEM investigations for Ni_5Sb_2 showed monodisperse particles of about 100 nm in diameter and agglomerated particles for NiSb (Figure 2b, d).

In the *Rh–Sb* system four room temperature phases Rh_2Sb, RhSb, $RhSb_2$, $RhSb_3$ and a high-temperature phase Rh_3Sb_2 are known.[54] RhSb nanoparticles can be obtained by sequential $NaBH_4$ reduction of $RhCl_3$ and $SbCl_3$.[55] Silica-supported Rh_2Sb and RhSb nanocatalysts were recently prepared by pore-filling impregnation of metal salts, drying, and reduction in a H_2 stream.[56,57] Starting from the metal acetates with an initial Rh:Sb ratio of 1:1 the intermetallic compound RhSb was obtained via the microwave-assisted polyol process (Figure 2e). EDS showed a composition $Rh_{46(1)}Sb_{54(1)}$ for the product, probably due to the phase width of RhSb or impurities not detectable by PXRD. The product consists of intergrown small platelets, which form star-shaped agglomerates with up to 200 nm in diameter (Figure 2f). Similar to the synthesis of β-Ni_3Sn_2, the polyol process generated a special product morphology. Moreover, the initial Rh:Sb ratio can be varied between 1:1 and 1:6 without altering the powder X-ray diffractogram and product morphology. Synthesis attempts towards Rh_2Sb and Rh_3Sb_2 resulted in mixtures of elemental rhodium and RhSb.

The *Pd–Sb* phase diagram exhibits six room-temperature ($Pd_{20}Sb_7$, Pd_8Sb_3, Pd_5Sb_2, Pd_2Sb, PdSb, $PdSb_2$) and two high-temperature compounds (Pd_3Sb, Pd_5Sb_3).[58] To the best of our knowledge, the only example of nanoparticle synthesis in this system was described by Schaak et al., who obtained Pd_8Sb_3 from reacting preformed Pd nanoparticles in a $SbCl_3$ solution with $NaBH_4$.[55] Using the microwave-assisted polyol process the palladium-rich compounds $Pd_{20}Sb_7$, Pd_8Sb_3 and PdSb could be obtained as phase-pure powders (Figure 2g, i, k). Only for the synthesis of the palladium-richest compound $Pd_{20}Sb_7$ (EDS analysis: expected $Pd_{74.1}Sb_{25.9}$; measured $Pd_{75.6(1)}Sb_{24.4(1)}$) the exactly matching initial ratio of the metal cations was essential. Pd_8Sb_3 (EDS analysis: expected $Pd_{72.7}Sb_{26.3}$; measured $Pd_{69.8(4)}Sb_{30.2(4)}$) was obtained from initial ratios Pd:Sb = 8:3 with the addition of KOH or 1:2 in pure ethylene glycol. PdSb without any solid byproduct (EDS analysis: $Pd_{51(1)}Sb_{49(1)}$) crystallized starting from the initial ratio Pd:Sb = 1:4.6 at 240 °C. Excess antimony cations remained in solution at this temperature. At 300 °C, the antimony-rich compound $PdSb_2$ was present as a byproduct (Figure S4 in the Supporting Information). The utilization of ethylene glycol and oleylamine in combination with KOH is crucial for the phase-pure formation of PdSb; otherwise mixtures with other Pd–Sb phases were observed. Due to the varying synthesis conditions, the size of the product particles is very different. Particles with diameters of about 30 nm for $Pd_{20}Sb_7$ (Figure 2h), 100 nm for Pd_8Sb_3 (Figure 2j), and 200 nm for PdSb (Figure 2l) were observed.

Synthesis of *T*–Pb phases. Contrary to tin and antimony, the reduction to elemental lead via an unmodified polyol process is possible. As a consequence, lead-rich intermetallic phases can easily be obtained. The systems Co–Pb, Ni–Pb, and Ir–Pb do not show any thermodynamically stable intermetallic phases and synthesis attempts yielded mixtures of monometallic products.

The phase diagram of the *Rh–Pb* system shows five room-temperature phases (Rh_3Pb_2, RhPb, Rh_4Pb_5, $RhPb_2$, $RhPb_4$).[59] Nanocrystalline Rh–Pb/SiO_2 catalysts (Rh_3Pb_2, RhPb, and $RhPb_2$) were prepared by co-impregnation of silica templates followed by H_2 reduction.[60] Using the microwave-assisted polyol process $RhPb_2$ could be obtained (Figure 3a). The product contains only small impurities of Rh_4Pb_5 and EDS analyses showed a composition $Rh_{35(2)}Pb_{65(2)}$, which is close to the expected value $Rh_{33.3}Pb_{66.7}$. Syntheses starting with a higher Rh amount in the reaction mixture yielded only poorly crystalline products. Similar to synthesis attempts in the Rh–Sn system, the small particle size due to a fast reduction of Rh^{2+} leads to weak diffraction signals.

The phase diagram of *Pd–Pb* contains five room-temperature phases (Pd_3Pb, α-Pd_5Pb_3, $Pd_{13}Pb_9$, PdPb, $PdPb_2$) and the high-temperature phase β-Pd_5Pb_3.[61] Nanocrystalline Pd_3Pb has already been obtained by borohydride reduction.[62,63] A two-step polyol process was used to produce carbon-supported Pd_3Pb nanoparticles.[25] α-Pb_5Pd_3 could be accessed by a sequential two-step reduction protocol with $NaBH_4$.[55] All Pd–Pb compounds except for the high-temperature phase β-Pd_5Pb_3 are accessible with the polyol process, but only in the case of Pd_3Pb as a phase-pure product. The powder pattern of Pd_3Pb exhibits broadened reflections (Figure 3c) due to a crystallite domain size of about 10 nm, according to Rietveld refinement. This is consistent with SEM pictures showing highly agglomerated small particles (Figure 3d). For the product α-Pb_5Pd_3 only trace impurities of $Pd_{13}Pb_9$ could be detected by PXRD (Figure S6 in the Supporting Information).

The phase diagram of *Pt–Pb* reveals three phases Pt_3Pb, PbPt and $PtPb_4$.[64] The synthesis of nanoscale PtPb was already achieved, e.g., by reduction of the metal salts with sodium borohydride[20,65] or sodium naphthalide[66].

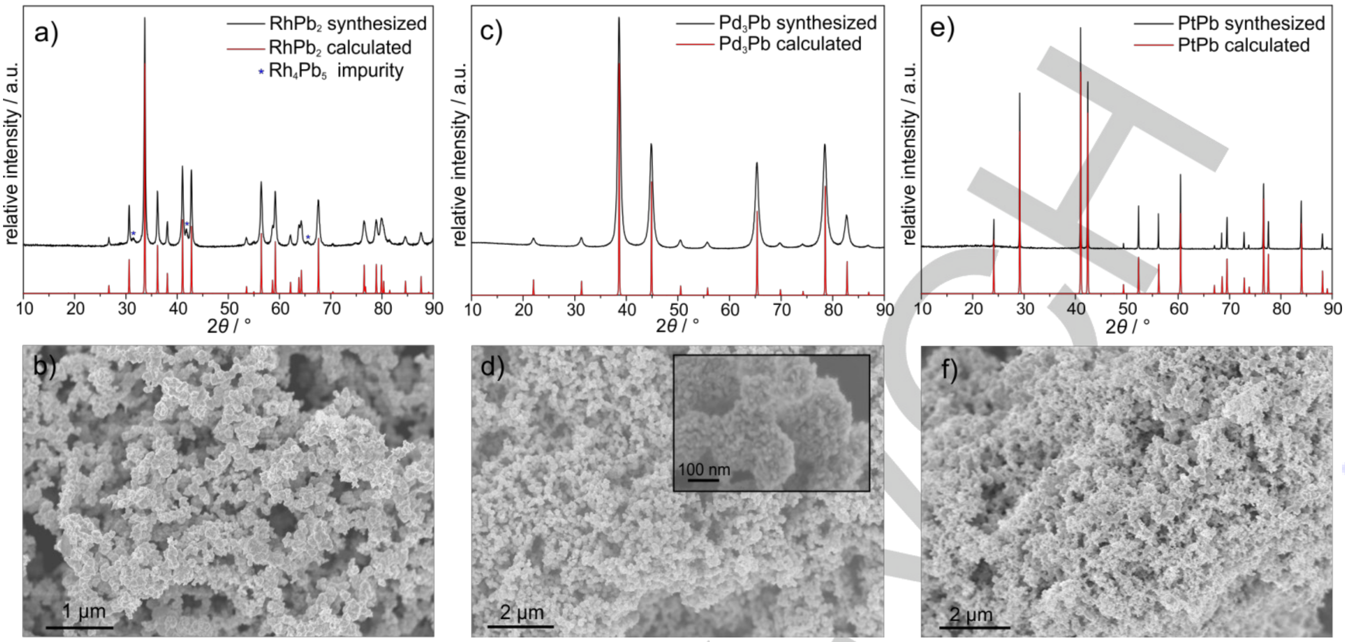

Figure 3. X-ray powder diffractograms (Cu-Kα1 radiation) and SEM pictures of (a, b) $RhPb_2$, (c, d) Pd_3Pb, and (e, f) PtPb, respectively. XRD shows Rh_4Pb_5 as a minor impurity for $RhPb_2$. According to the SEM pictures agglomerated nanoparticles were obtained.

Furthermore, the formation of PtPb nanorods by *tert*-butylamine borane in a mixture of diphenyl ether, adamantine carboxylic acid, hexadecanethiol, and hexadecylamine at 180 °C was described.[67] A two-step synthesis protocol for PtPb nanoparticles on a WO_3 substrate, comprising the photodeposition of Pt nanoparticles on WO_3 and subsequent polyol reduction of Pb^{2+}, was reported recently.[68] With the microwave-assisted polyol process, PbPt was obtained in a single step as highly crystalline particles with diameters up to 200 nm (Figure 3e, f). Starting with a high initial amount of Pb^{2+} mixtures of PtPb and $PtPb_4$ were obtained.

Synthesis of PtBi and $PtBi_2$. The Pt–Bi phase diagram hosts two compounds that are stable at room-temperature (PtBi, α-$PtBi_2$) and three high-temperature phases (Pt_2Bi_3, β-$PtBi_2$, and γ-$PtBi_2$).[69] Additionally, a third high-temperature phase of $PtBi_2$ (δ-phase) has been mentioned, whereas its existence is not clarified yet.[69] Some syntheses of nanocrystalline Pt–Bi compounds have already been published. Schaak et al. described the synthesis of nanoscale PtBi by the co-reduction of bismuth(III) nitrate pentahydrate and potassium hexachloridoplatinate(IV) in tetraethylene glycol with $NaBH_4$ and poly(vinylpyrrolidone) at 220 °C.[20] The DiSalvo group achieved the synthesis of PtBi by using ethylene glycol as the only reducing agent.[27] However, the synthesis protocol includes the use of an inert gas atmosphere and the total synthesis time is about three days. Depending on the reaction temperature, PtBi and γ-$PtBi_2$ nanoparticles were produced in a continuous flow setup.[26] Increasing the temperature to 350 °C led to phase-pure trigonal γ-$PtBi_2$, whereas at lower temperatures PtBi or mixtures of PtBi and Pt occurred.

We synthesized phase-pure PtBi with the microwave-assisted polyol process (Figure 4). SEM of the PtBi product revealed a homogeneous powder of rather isotropic particles (diameter about 50 nm) and smaller fibrous particles decorating their surface. In EDS analyses, the composition of the powder samples was determined as $Pt_{50.5(5)}Bi_{49.5(5)}$. PXRD verified the previously assigned NiAs structure type. The lattice parameters determined by Rietveld refinement (*a* = 433.1 pm and *c* = 550.4 pm) are slightly higher than those reported in the literature (*a* = 431.5 pm, *c* = 549 pm).[70] This could be due to a phase width of PtBi at least in its nanocrystalline form, which cannot be seen in the phase diagram. The existence of phase widths is known to be a common characteristic of NiAs-type intermetallics.[71] Likewise, Pt_2Bi_3 is a defective variant of the NiAs structure type. This high-temperature phase is thermodynamically stable above 570 °C as bulk material. It can be obtained as a byproduct besides PtBi and γ-$PtBi_2$ starting from an initial Pt:Bi ratio of 2:3.

The synthesis of $PtBi_2$ resulted in the simultaneous formation of the three known modifications α, β, and γ. High-temperature phases were obtained at 240 °C, which is below their bulk formation temperatures (β-$PtBi_2$: 272 °C, γ-$PtBi_2$: 420 °C). Rietveld refinement of the phase fractions revealed a reaction time dependency of the phase distribution (Figure S8 and Table S2 in the Supporting Information). With a reaction time of 5 min the distribution is α:β:γ = 14:14:72 wt.-%. After 30 min it changes to 26:28:46 wt.-% and after 60 min to 45:47:8 wt.-%.

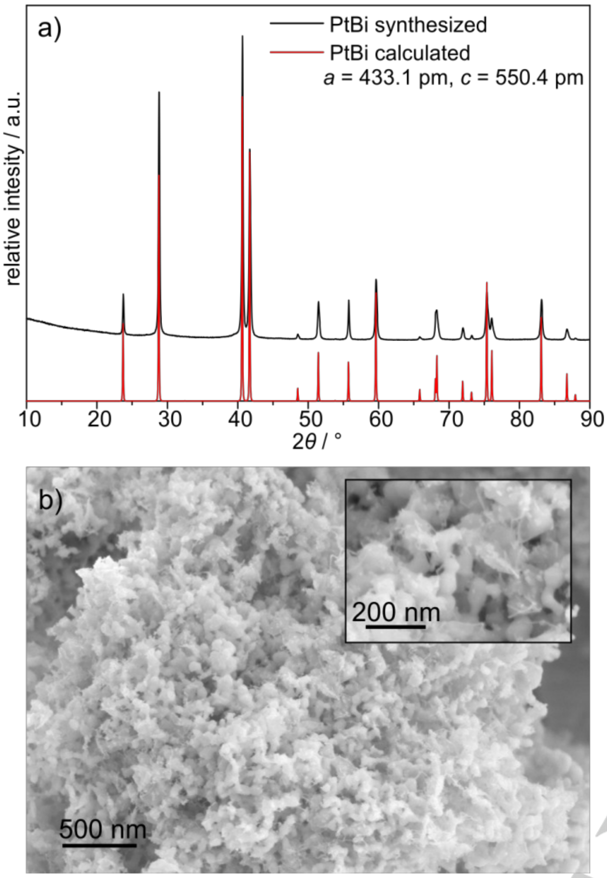

Figure 4. X-ray powder diffractogram (Cu-K$_{\alpha1}$ radiation; a) and SEM pictures (b) of phase-pure PtBi.

The longer the reaction mixtures are annealed at 240 °C the more of the α- and β-form are obtained and the amount of the γ-modification decreases. This can be explained by Ostwald's step rule, which states that the least-stable modification of a compound would occur first during a crystallization process. Accordingly, the γ-$PtBi_2$ should be the least stable form and transforms to β-$PtBi_2$, which is also metastable at the reaction conditions, and finally to the thermodynamically stable α-$PtBi_2$. Remarkably, the phase fractions of α- and β-$PtBi_2$ have a ratio of approximately 1:1 over the entire reaction time. β-$PtBi_2$ seems to be stabilized under the reaction conditions, since the phase transition temperature of 272 °C is not much higher than the reaction temperature of 240 °C. It has to be taken into account, that phase transition temperatures can be significantly decreased in nanostructured systems.[1]

Conclusions

We demonstrated the power of the microwave-assisted polyol process as a feasible method for the synthesis of a wide range of binary nanocrystalline intermetallics in the systems T–M (T = Co, Ni, Rh, Pd, Ir, Pt; M = Sn, Sb, Pb, Bi). Ethylene glycol was utilized as a solvent and reducing agent without adding stronger reducing agents. Phase formation takes place at comparatively low temperatures within minutes. To crystallize as many phases as possible we had to optimize the synthesis procedures by adding KOH, oleylamine, and oleic acid.

A variety of phase-pure powders was obtained: β-Ni_3Sn_2, Pd_2Sn, $Pd_{20}Sn_{13}$, PdSn, Pt_3Sn, PtSn, CoSb, Ni_5Sb_2, NiSb, $Pd_{20}Sb_7$, Pd_8Sb_3, PdSb, Pd_3Pb, PtPb, and PtBi. Synthesis protocols for some of these compounds in nanocrystalline form have already been known, but there are some disadvantages like toxic and corrosive reducing agents, long reaction times, necessity of inert gas protection, or the need for multi-step processes. With the microwave-assisted polyol process, intermetallic compounds can be synthesized in one step and in a comparatively short time, using less toxic solvents and no inert gas. For the first time, we presented the synthesis of nanostructured single-phase samples of Ni_5Sb_2, $Pd_{20}Sb_7$, and PdSb. In the cases of β-Ni_3Sn, β-Ni_3Sn_2, β-/γ-$PtBi_2$, and Pt_2Bi_3 the crystallization and stabilization of high-temperature phases was observed at temperatures below their bulk formation temperature, similar to the previously reported syntheses in the Pd–Bi system.[31]

Furthermore, we identified some limitations of the method. The crystallization of bismuth- or lead-rich phases is in general possible, whereas antimony- and tin-rich phases seem to be not accessible with the presented method. In most phase systems, only particular phases can be crystallized, especially in the case of antimony- or tin-containing compounds. The intermetallic phase formation itself seems to be an essential driving force for the reduction of Sb^{3+} and Sn^{2+}, which is confirmed by the non-reactivity of these cations themselves in ethylene glycol, even at 300 °C.

Experimental Section

Chemicals. For synthesis of the nanocrystalline intermetallic compounds all chemicals were used as received from the supplier. Metal salts and solvents for synthesis: cobalt(II) nitrate hexahydrate (99 %, Merck), nickel(II) acetate tetrahydrate (99 %, Merck), rhodium(II) acetate (99 %, ABCR), palladium(II) acetate (48.35 % Pd, ABCR), platinum(II) acetylacetonate (49.6 % Pt, ChemPur), tin(II) acetate (p.a., Sigma Aldrich), antimony(III)-acetate (97 %, Alfa Aesar), lead(ii) acetate trihydrate (Sigma-Aldrich, 99.5 %), lead(II) nitrate (p.a., Riedel-de Haën), bismuth(III) acetate (abcr, 99 %), bismuth(III) nitrate pentahydrate (98.5 %, Riedel-de Haën), potassium hydroxide (analytical reagent grade, Fischer Chemical), ethylene glycol (99.5 %, Fluka), oleylamine (technical grade 70 %, Sigma-Aldrich), oleic acid (pure, AppliChem).

Synthesis. The nanocrystalline intermetallic compounds were synthesized by microwave-assisted polyol process in a CEM Discover SP synthesis microwave, which allows monitoring of the reaction by a video camera. Ethylene glycol was used as solvent and reducing agent. We used KOH to modify the pH, what can have a significant impact on the reducibility of the metal salts. All reactions were carried out in 35 ml Pyrex® vessels equipped with magnetic stirring bars ensuring proper mixing of the reagents. Specific synthesis conditions can be found in Table S1 in the Supporting Information. The metal salts and KOH, if necessary, were dissolved in 15 ml of EG. The reaction mixtures were heated to the desired temperature in 3 min using microwave radiation. After annealing for up to 60 min, the vessels were cooled with a stream of air to 60 °C inside the microwave device and then removed. The black powdery products were isolated by centrifugation, washed several times with ethanol or acetone to remove residual solvent, and dried overnight under vacuum at room temperature. Yields of the products regularly exceed 90 %.

Characterization. X-ray powder diffractograms were recorded at 296(2) K on an X'Pert Pro MPD diffractometer (PANalytical) equipped with a curved Ge(111) monochromator using Cu-K$_{\alpha1}$ radiation (λ = 154.056 pm). Rietveld refinement was performed with TOPAS, using the fundamental parameter approach and spherical harmonics functions for modelling preferred orientation.[72] Scanning electron microscopy was carried out using a SU8020 (Hitachi) with a triple detector system for secondary and low-energy backscattered electrons (U = 3 kV). A Silicon Drift Detector X-Max^N (Oxford) was used to perform energy dispersive X-ray spectroscopy for semi-quantitative composition analysis. Cold pressed pellets of the nanocrystalline powders were fixed on silicon wafers to produce a plane surface for the measurement.

Acknowledgements

We gratefully acknowledge Alexander Weiz for assistance with EDS investigations. This work was supported by the Deutsche Forschungsgemeinschaft (DFG).

Keywords: Nanoparticles • Intermetallic phases • Microwave chemistry • Polyol process

[1] E. Roduner, *Chem. Soc. Rev.* **2006**, *35*, 583–592.
[2] K. D. Gilroy, A. Ruditskiy, H.-C. Peng, D. Qin, Y. Xia, *Chem. Rev.* **2016**, *116*, 10414–10472.
[3] Y. Yan, J. S. Du, K. D. Gilroy, D. Yang, Y. Xia, H. Zhang, *Adv. Mater.* **2017**, *29*, 1605997.
[4] R. Pöttgen, D. Johrendt, *Intermetallics: Synthesis, Structure, Function*, De Gruyter, Berlin, **2014**.
[5] M. Figlarz, F. Fiévet, J.-P. Lagier, *Process for the Reduction of Metallic Compounds by Polyols, and Metallic Powders Obtained by This Process*, **1985**, US 4539041 A.
[6] F. Fiévet, J. P. Lagier, B. Blin, B. Beaudoin, M. Figlarz, *Solid State Ion.* **1989**, *32–33*, 198–205.
[7] F. Fiévet, J.-P. Lagier, M. Figlarz, *MRS Bull.* **1989**, *14*, 29–34.
[8] H. Dong, Y.-C. Chen, C. Feldmann, *Green Chem.* **2015**, *17*, 4107–4132.
[9] F. Bonet, C. Guéry, D. Guyomard, R. Herrera Urbina, K. Tekaia-Elhsissen, J.-M. Tarascon, *Int. J. Inorg. Mater.* **1999**, *1*, 47–51.
[10] C. Ducamp-Sanguesa, R. Herrera-Urbina, M. Figlarz, *J. Solid State Chem.* **1992**, *100*, 272–280.
[11] C. Ducamp-Sanguesa, R. Herrera-Urbina, M. Figlarz, *Solid State Ion.* **1993**, *63*, 25–30.
[12] S. Komarneni, D. Li, B. Newalkar, H. Katsuki, A. S. Bhalla, *Langmuir* **2002**, *18*, 5959–5962.
[13] W. Z. Wang, B. Poudel, Y. Ma, Z. F. Ren, *J. Phys. Chem. B* **2006**, *110*, 25702–25706.
[14] K. J. Carroll, J. U. Reveles, M. D. Shultz, S. N. Khanna, E. E. Carpenter, *J. Phys. Chem. C* **2011**, *115*, 2656–2664.
[15] C. Kind, C. Feldmann, *Chem. Mater.* **2011**, *23*, 4982–4987.
[16] K. M. Koczkur, S. Mourdikoudis, L. Polavarapu, S. E. Skrabalak, *Dalton Trans.* **2015**, *44*, 17883–17905.
[17] S. Mourdikoudis, L. M. Liz-Marzán, *Chem. Mater.* **2013**, *25*, 1465–1476.
[18] A. K. Sra, R. E. Schaak, *J. Am. Chem. Soc.* **2004**, *126*, 6667–6672.
[19] A. K. Sra, T. D. Ewers, R. E. Schaak, *Chem. Mater.* **2005**, *17*, 758–766.
[20] R. E. Cable, R. E. Schaak, *Chem. Mater.* **2005**, *17*, 6835–6841.
[21] N. H. Chou, R. E. Schaak, *J. Am. Chem. Soc.* **2007**, *129*, 7339–7345.
[22] B. M. Leonard, N. S. P. Bhuvanesh, R. E. Schaak, *J. Am. Chem. Soc.* **2005**, *127*, 7326–7327.
[23] B. M. Leonard, R. E. Schaak, *J. Am. Chem. Soc.* **2006**, *128*, 11475–11482.
[24] D. Sun, L. Si, G. Fu, C. Liu, D. Sun, Y. Chen, Y. Tang, T. Lu, *J. Power Sources* **2015**, *280*, 141–146.
[25] T. Gunji, S. H. Noh, T. Tanabe, B. Han, C. Y. Nien, T. Ohsaka, F. Matsumoto, *Chem. Mater.* **2017**, *29*, 2906–2913.
[26] D. Zhang, F. Wu, M. Peng, X. Wang, D. Xia, G. Guo, *J. Am. Chem. Soc.* **2015**, *137*, 6263–6269.
[27] C. Roychowdhury, F. Matsumoto, P. F. Mutolo, H. D. Abruña, F. J. DiSalvo, *Chem. Mater.* **2005**, *17*, 5871–5876.
[28] R. Boldt, A. Grigas, M. Heise, T. Herrmannsdörfer, A. Isaeva, S. Kaskel, D. Köhler, M. Ruck, R. Skrotzki, J. Wosnitza, *Z. anorg. allg. Chem.* **2012**, *638*, 2035–2043.
[29] D. Köhler, M. Heise, A. I. Baranov, Y. Luo, D. Geiger, M. Ruck, M. Armbrüster, *Chem. Mater.* **2012**, *24*, 1639–1644.
[30] M. Heise, B. Rasche, A. Isaeva, A. I. Baranov, M. Ruck, K. Schäfer, R. Pöttgen, J.-P. Eufinger, J. Janek, *Angew. Chem.* **2014**, *126*, 7472–7476; *Angew. Chem. Int. Ed.* **2014**, *53*, 7344–7348.
[31] M. Heise, J.-H. Chang, R. Schönemann, T. Herrmannsdörfer, J. Wosnitza, M. Ruck, *Chem. Mater.* **2014**, *26*, 5640–5646.
[32] I. Bilecka, M. Niederberger, *Nanoscale* **2010**, *2*, 1358–1374.
[33] M. Baghbanzadeh, L. Carbone, P. D. Cozzoli, C. O. Kappe, *Angew. Chem.* **2011**, *123*, 11510–11561; *Angew. Chem. Int. Ed.* **2011**, *50*, 11312–11359.
[34] Y.-J. Zhu, F. Chen, *Chem. Rev.* **2014**, *114*, 6462–6555.
[35] T. Herrmannsdörfer, R. Skrotzki, J. Wosnitza, D. Köhler, R. Boldt, M. Ruck, *Phys. Rev. B* **2011**, *83*, 140501.
[36] X. Zhu, H. Lei, C. Petrovic, Y. Zhang, *Phys. Rev. B* **2012**, *86*, 024527.
[37] G. Viau, F. Fiévet-Vincent, F. Fiévet, *J. Mater. Chem.* **1996**, *6*, 1047–1053.
[38] R. J. Joseyphus, D. Kodama, T. Matsumoto, Y. Sato, B. Jeyadevan, K. Tohji, *J. Magn. Magn. Mater.* **2007**, *310*, 2393–2395.
[39] R. J. Joseyphus, K. Shinoda, D. Kodama, B. Jeyadevan, *Mater. Chem. Phys.* **2010**, *123*, 487–493.
[40] H. Okamoto, *J. Phase Equilib. Diffus.* **2008**, *29*, 297–298.
[41] H. Qin, X. Zhao, N. Jiang, Z. Li, *J. Power Sources* **2007**, *171*, 948–952.
[42] X.-L. Wang, W.-Q. Han, J. Chen, J. Graetz, *ACS Appl. Mater. Interfaces* **2010**, *2*, 1548–1551.
[43] H. Okamoto, *J. Phase Equilib. Diffus.* **2012**, *33*, 253–254.
[44] C. Wang, Y. Wu, X. Wang, L. Zou, Z. Zou, H. Yang, *Electrochim. Acta* **2016**, *220*, 628–634.
[45] V. Grolier, R. Schmid-Fetzer, *J. Alloys Compd.* **2008**, *450*, 264–271.
[46] D. Y. DeSario, F. J. DiSalvo, *Chem. Mater.* **2014**, *26*, 2750–2757.
[47] X. Wang, L. Altmann, J. Stöver, V. Zielasek, M. Bäumer, K. Al-Shamery, H. Borchert, J. Parisi, J. Kolny-Olesiak, *Chem. Mater.* **2013**, *25*, 1400–1407.
[48] D. O. Downing, Z. Liu, B. W. Eichhorn, *Polyhedron* **2016**, *103*, 66–70.
[49] Y. Zhang, C. Li, Z. Du, C. Guo, *Calphad* **2008**, *32*, 378–388.
[50] C. Li, J. Hu, Q. Peng, X. Wang, *Mater. Chem. Phys.* **2008**, *110*, 106–109.
[51] L. Kumari, W. Li, J. Y. Huang, P. P. Provencio, *J. Phys. Chem. C* **2010**, *114*, 9573–9579.
[52] P. P. Shanbogh, S. C. Peter, *RSC Adv.* **2013**, *3*, 22887.
[53] G. Kieslich, C. S. Birkel, A. Stewart, U. Kolb, W. Tremel, *Inorg. Chem.* **2011**, *50*, 6938–6943.
[54] H. Okamoto, in *Binary Alloy Phase Diagrams, Second Edition* (Ed.: T.B. Massalski), ASM International, Materials Park, Ohio, USA, **1990**, pp. 3223–3225.
[55] B. M. Leonard, M. E. Anderson, K. D. Oyler, T.-H. Phan, R. E. Schaak, *ACS Nano* **2009**, *3*, 940–948.
[56] S. Furukawa, A. Yokoyama, T. Komatsu, *ACS Catal.* **2014**, *4*, 3581–3585.

[57] S. Furukawa, K. Ochi, H. Luo, M. Miyazaki, T. Komatsu, *ChemCatChem* **2015**, *7*, 3472–3479.

[58] W. Han, M. Li, *J. Alloys Compd.* **2010**, *507*, 521–525.

[59] H. Okamoto, in *Binary Alloy Phase Diagrams–Second Edition* (Ed.: T.B. Massalski), ASM International, Materials Park, Ohio, USA, **1990**, pp. 3005–3007.

[60] S. Furukawa, K. Takahashi, T. Komatsu, *Chem Sci.* **2016**, *7*, 4476–4484.

[61] H. Okamoto, *J. Phase Equilib.* **1997**, *18*, 491.

[62] Z. Cui, H. Chen, M. Zhao, F. J. DiSalvo, *Nano Lett.* **2016**, *16*, 2560–2566.

[63] R. Jana, U. Subbarao, S. C. Peter, *J. Power Sources* **2016**, *301*, 160–169.

[64] Z. H. Long, X. M. Tao, H. S. Liu, Z. P. Jin, *J. Phase Equilib. Diffus.* **2009**, *30*, 318–322.

[65] C. Roychowdhury, F. Matsumoto, V. B. Zeldovich, S. C. Warren, P. F. Mutolo, M. Ballesteros, U. Wiesner, H. D. Abruña, F. J. DiSalvo, *Chem. Mater.* **2006**, *18*, 3365–3372.

[66] L. R. Alden, D. K. Han, F. Matsumoto, H. D. Abruña, F. J. DiSalvo, *Chem. Mater.* **2006**, *18*, 5591–5596.

[67] S. Maksimuk, S. Yang, Z. Peng, H. Yang, *J. Am. Chem. Soc.* **2007**, *129*, 8684–8685.

[68] T. Gunji, A. J. Jeevagan, M. Hashimoto, T. Nozawa, T. Tanabe, S. Kaneko, M. Miyauchi, F. Matsumoto, *Appl. Catal., B* **2016**, *181*, 475–480.

[69] H. Okamoto, *J. Phase Equilib.* **1991**, *12*, 207–210.

[70] N. N. Zhuravlev, A. A. Stepanova, *Kristallografiya* **1962**, *7*, 310–11.

[71] S. Lidin, A.-K. Larsson, *J. Solid State Chem.* **1995**, *118*, 313–322.

[72] A. Coelho, *TOPAS-Academic V5*, Brisbane, Australia, **2012**.

Entry for the Table of Contents (Please choose one layout)

FULL PAPER

A variety of binary intermetallic phases was synthesized with the microwave-assisted polyol process. This approach opens up the possibility to obtain phase-pure nanocrystalline powders in a fast and easily applicable one-step route. Ethylene glycol was used as solvent and reducing agent. The utilization of strong and often toxic reducing agents is not necessary.

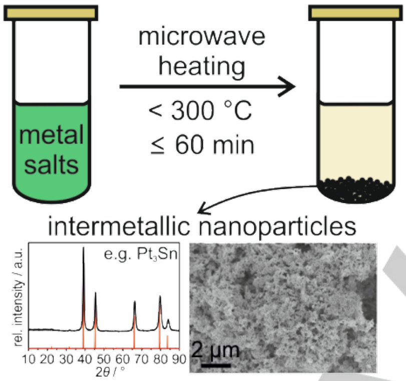

Intermetallic Nanoparticles

*Johannes Teichert, Martin Heise, Jen-Hui Chang, Michael Ruck**

Page No. – Page No.

Evaluation of the Microwave-Assisted Polyol Process for the Synthesis of Intermetallic Nanoparticles